The Journal of Chemical Physics

RESEARCH ARTICLE | APRIL 26 2024

Structural dynamics of the heme pocket and intersubunit coupling in the dimeric hemoglobin from *Scapharca inaequivalvis* FREE

Special Collection: Time-resolved Vibrational Spectroscopy

Xiang Gao ; Misao Mizuno ; Haruto Ishikawa ; Srinivasan Muniyappan ; Hyotcherl Ihee ; Yasuhisa Mizutani

J. Chem. Phys. 160, 165102 (2024)
https://doi.org/10.1063/5.0203594
CHORUS

AIP Publishing

The Journal of Chemical Physics ARTICLE pubs.aip.org/aip/jcp

Structural dynamics of the heme pocket and intersubunit coupling in the dimeric hemoglobin from *Scapharca inaequivalvis*

Cite as: J. Chem. Phys. 160, 165102 (2024); doi: 10.1063/5.0203594
Submitted: 15 February 2024 • Accepted: 8 April 2024 •
Published Online: 26 April 2024

Xiang Gao,[1] Misao Mizuno,[1,a)] Haruto Ishikawa,[1] Srinivasan Muniyappan,[2,3,b)] Hyotcherl Ihee,[2,3] and Yasuhisa Mizutani[1,c)]

AFFILIATIONS

[1] Department of Chemistry, Graduate School of Science, Osaka University, 1-1 Machikaneyama, Toyonaka, Osaka 560-0043, Japan
[2] Department of Chemistry and KI for the BioCentury, KAIST, Daejeon 305-701, Republic of Korea
[3] Center for Advanced Reaction Dynamics, Institute for Basic Science (IBS), Daejeon 305-701, Republic of Korea

Note: This paper is part of the JCP Special Topic on Time-Resolved Vibrational Spectroscopy 2023.
[a)] **Present address:** Department of Chemistry, Graduate School of Science, Kyoto University, Kitashirakawa-Oiwakecho, Sakyo-ku, Kyoto 606-8502, Japan.
[b)] **Present address:** Department of Physics, University of Wisconsin-Milwaukee, Milwaukee, WI 53211, USA.
[c)] **Author to whom correspondence should be addressed:** mztn@chem.sci.osaka-u.ac.jp

ABSTRACT

Cooperativity is essential for the proper functioning of numerous proteins by allosteric interactions. Hemoglobin from *Scapharca inaequivalvis* (HbI) is a homodimeric protein that can serve as a minimal unit for studying cooperativity. We investigated the structural changes in HbI after carbon monoxide dissociation using time-resolved resonance Raman spectroscopy and observed structural rearrangements in the Fe–proximal histidine bond, the position of the heme in the pocket, and the hydrogen bonds between heme and interfacial water upon ligand dissociation. Some of the spectral changes were different from those observed for human adult hemoglobin due to differences in subunit assembly and quaternary changes. The structural rearrangements were similar for the singly and doubly dissociated species but occurred at different rates. The rates of the observed rearrangements indicated that they occurred synchronously with subunit rotation and are influenced by intersubunit coupling, which underlies the positive cooperativity of HbI.

I. INTRODUCTION

Protein cooperativity due to allosteric interactions is essential for the proper functioning of many proteins and has thus been a topic of intense study.[1–3] For such cooperativity, the affinity for a ligand at multiple binding sites is either increased (positive cooperativity) or decreased (negative cooperativity) upon binding of the ligand to a binding site. Cooperativity is crucial to the functions of enzymes and transporter proteins, but elucidating the mechanism of protein cooperativity remains challenging.

Hemoglobin is a paradigmatic protein showing cooperativity and has played a pivotal role in aiding our understanding of the mechanisms of cooperativity. Human adult hemoglobin (HbA) is composed of two α and two β subunits, with each subunit containing a heme cofactor as the oxygen-binding site.[4–7] HbA exhibits positive cooperativity in oxygen binding. The static protein structures of the oxy and deoxy forms have been determined by x-ray crystallographic studies,[8,9] whereas the dynamics of the HbA structure have been studied by utilizing the rapid dissociation of the ligand (in less than 100 fs) upon the photoexcitation of the ligand-bound heme.[10,11] Carbon monoxide (CO) is typically used for studies on HbA dynamics because the quantum yield of the photodissociation is almost unity,[12,13] and autoxidation can be avoided. Geminate rebinding of CO to heme proteins greatly differs from that of O_2.[14–16] Generally, the amplitude and rate of the geminate rebinding of CO are smaller and lower than those of O_2, making it advantageous for observations of protein dynamics following the ligand dissociation. Time-resolved resonance Raman (RR) spectroscopy

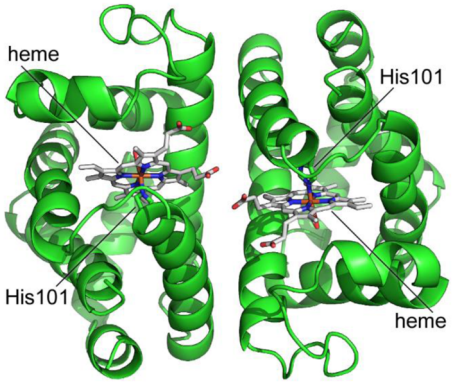

FIG. 1. Protein structure of deoxy HbI (PDB ID: 4SDH).

has been utilized to observe structural changes in heme[17–19] and in globin, including in the subunit interface.[20–27] Time-resolved RR spectroscopy allowed the identification of intermediates following ligand dissociation and revealed the mechanism underlying the quaternary transition of HbA.[26–30]

The dependence of protein dynamics on the number of dissociated ligands in hemoglobins is intriguing because it provides insight into the interactions between subunits, and these interactions underlie cooperativity. However, this dependence is difficult to study in the HbA tetramer because it is composed of two non-identical subunits, giving rise to a large number of possible partially dissociated HbA species. In contrast, HbI from *Scapharca inaequivalvis* is a homodimeric hemoglobin (Fig. 1), and oxygen binding is cooperative.[31] Thus, HbI represents a minimal system for studying the cooperativity of hemoglobins, including the dependence of protein dynamics on the number of dissociated ligands.

The x-ray crystallographic studies unveiled the equilibrium protein structures of the ligated and deligated forms of HbI. Structural differences between the forms were determined for the heme group, heme pocket, and assembly of the subunits.[32–38] Notably, the rotational angle of one subunit relative to the second subunit differed by 3.4° between the carbon monoxide (CO)-bound and deoxy forms,[33] and the arrangement of the water molecules at the subunit interface also differed.[34–36] Transient absorption studies revealed that the structure of the heme changed within microseconds following the dissociation of CO from the CO-bound form of HbI.[39–41] The dynamics of the quaternary structure of HbI was studied using time-resolved x-ray solution scattering, also known as time-resolved x-ray liquidography (TRXL).[42–47] One subunit was observed to rotate relative to the second subunit by 3.4° in the microsecond time range. Previous time-resolved studies reported that the kinetics of the structural changes following CO dissociation differ between the singly and doubly dissociated forms of HbI,[39,42] which led to detailed studies on the static HbI structures and on its quaternary dynamics following CO dissociation. However, the structural dynamics of the heme group and heme pocket, coupled with the dynamics of the quaternary structure, remained poorly understood.

Herein, we report a time-resolved RR study following CO photodissociation in HbI. The spectra showed changes in the position of heme relative to the heme pocket, in the iron–proximal histidine bond, and in hydrogen bonds between the heme propionate groups with nearby residues and interfacial water. The spectral changes were faster for doubly dissociated HbI than for singly dissociated HbI, showing that the structural changes in the heme pocket and in the subunits are coupled. The rates of the observed spectral changes were similar to that of the change in the quaternary structure, indicating that the structural rearrangements of the heme and heme pocket are almost synchronous with the relative rotation of the subunits. Discussion on the structural changes in the heme pocket of the two subunits in HbI focuses on the coupling between these changes.

II. EXPERIMENTAL METHODS

A. Protein expression and purification

Recombinant wild-type (WT) HbI from *Scapharca inaequivalvis* and its site-directed mutants were expressed in *E. coli* strain BL21 (DE3).[38,48] Site-directed mutagenesis was performed using PrimeStar Max methods (Takara Bio). The F97Y mutation was introduced using the primers 5′-GAA AAA TAT GCT GTT AAC CAT ATC ACG-3′ and 5′-AAC AGC ATA TTT TTC AAC AAC ACA AAC-3′. The F97L mutation was introduced using the primers 5′-GAA AAA CTG GCT GTT AAC CAT ATC ACG-3′ and 5′-AAC AGC CAG TTT TTC AAC AAC ACA AAC-3′. The WT and mutant HbI samples were purified according to the protocols described previously.[38,48]

B. Time-resolved resonance Raman measurements

The protein concentration of the sample solutions was set to 75 μM in 0.1M phosphate buffer at pH = 7.0 before the time-resolved RR measurements. The buffer contained 300 mM sodium sulfate as an internal intensity standard. The sample solution was placed in an airtight Ø10 mm nuclear magnetic resonance (NMR) tube under a CO or N_2 atmosphere to prepare the CO-bound and deoxy forms, respectively. Sodium dithionate solution (100 mM, 10 μl) was added to 1 ml of the sample solution to reduce the residual oxygen dissolved in the sample solutions and the heme iron, and then, the sample was spun at 3000 rpm. The experimental apparatus for time-resolved RR spectroscopy has been reported elsewhere.[49] The 442 nm probe pulse was the second harmonic of a Ti:sapphire laser (Photonics Industries, TU-L). The energy of the probe light was 0.3 μJ/pulse to minimize ligand photodissociation. The 532 nm pump pulses were generated with a diode-pumped Nd:YAG laser (Megaopto, LR-SHG), and the energy of the pump light was varied from 10 to 350 μJ/pulse to photodissociate CO from the protein in various yields. The two pulse lasers were operated at 1 kHz. The delay time between the pump and probe beams was adjusted by a computer-controlled digital delay generator (Stanford Research System, DG535), and the instrumental response time was about 50 ns. The scattered light was collected and focused onto the entrance slit of a Czerny–Turner configured Littrow prism prefilter (Bunkoukeiki, PF-200MP) coupled with a spectrograph (HORIBA Jobin Yvon, iHR550) and detected with a CCD camera (Roper Scientific, SPEC-10:400B/LN-SN-U). The Raman shift was calibrated using the Raman bands of cyclohexane, toluene, and carbon tetrachloride.

III. RESULTS AND DISCUSSION

A. Time-resolved RR spectra of photodissociated WT HbI

Figure 2(a) shows the time-resolved RR spectra of HbI obtained using a 300 μJ pump for CO dissociation and the RR spectra of the CO-bound and deoxy forms of HbI for comparison. The time-resolved RR spectra were obtained by subtraction of a spectral component of the CO-bound form from the raw pump–probe spectra. The spectral component of the CO-bound form involves contributions from the unphotolyzed species and geminately rebound species within the instrument response time. At 20 ns, the photodissociated HbI exhibited RR bands at 209, 301, 335, 365, 411, 672, 758, and 787 cm^{-1}, assigned to the ν(Fe–His), γ_7, γ_6, $\delta(C_\beta C_c C_d)$, $\delta(C_\beta C_a C_b)$, ν_7, ν_{16}, and ν_{32} modes, respectively.[50–55] The band assignments are summarized in Table I. The frequencies and intensities of the RR bands changed as the delay time increased, with the frequencies of the ν(Fe–His), ν_7, and ν_{16} bands showing a downshift and the $\delta(C_\beta C_c C_d)$ band exhibiting an upshift. The intensities of the ν_{16} and ν_{32} modes decreased and increased, respectively. An RR band appeared at 346 cm^{-1} at 10 μs but was absent at 20 ns. This band was assigned to the ν_8 mode. At 10 μs, the time-resolved RR spectrum was identical to that of the deoxy form reported previously

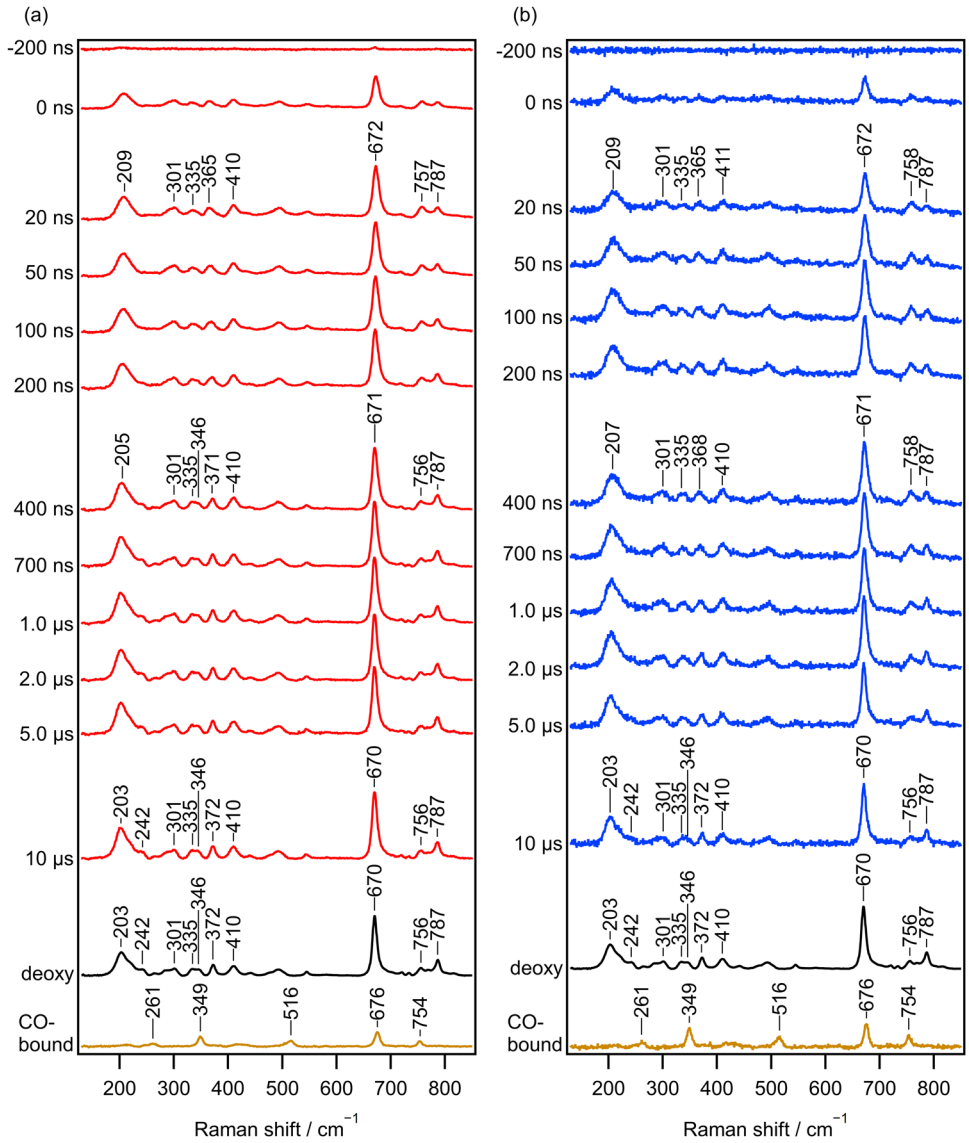

FIG. 2. Time-resolved RR spectra of WT HbI photodissociated under 300 μJ (a) and 10 μJ pumping conditions (b). The RR spectra of the CO-bound and deoxy forms of HbI are shown for comparison. The time-resolved spectra were generated by subtracting the probe-only spectrum from the pump–probe spectrum at each delay time.

TABLE I. Band assignments for the Raman bands of HbI.

Raman shift (cm^{-1})	Assignment[54,55]	Description
Deoxy form		
203	ν(Fe–His)	Iron–proximal histidine stretching
242	ν_9	Pyrrole ring–methyl bending coupled with
301	γ_7	Methine out-of-plane wagging pyrrole ring–propionate bending
335	γ_6	Pyrrole tilting
346	ν_8	Iron–pyrrole ring stretching
372	$\delta(C_\beta C_c C_d)$	Propionate methylene bending
410	$\delta(C_\beta C_a C_b)$	Vinyl bending
670	ν_7	Symmetric pyrrole ring deformation
756	ν_{16}	Symmetric pyrrole ring deformation
787	ν_{32}	Asymmetric pyrrole ring deformation
CO-bound form		
261	ν_9	Pyrrole ring–methyl bending coupled with pyrrole ring–propionate bending
349	ν_8	Iron–pyrrole ring stretching
516[b]	ν(Fe–CO)	Iron–carbon monoxide stretching
676	ν_7	Symmetric pyrrole ring deformation
754	ν_{16}	Symmetric pyrrole ring deformation

by Rousseau *et al.*[54] The spectrum at −200 ns was completely featureless, implying that no photoproducts were accumulated in the samples.

Figure 2(b) shows the time-resolved RR spectra of HbI obtained using a 10 μJ pump for CO dissociation. The RR spectrum at 20 ns at 10 μJ pumping condition [Fig. 2(b)] is similar to that at 20 ns at 300 μJ pumping condition [Fig. 2(a)], whereas the RR spectrum at 400 ns at 10 μJ pumping condition differs from that at 300 μJ pumping condition. The frequencies of the ν(Fe–His) and ν_{16} bands at 300 μJ pumping condition were lower than those at 10 μJ pumping condition. Conversely, the frequency of the $\delta(C_\beta C_c C_d)$ band at 300 μJ pumping condition was higher than that at 10 μJ pumping condition. These differences indicate that the temporal changes in the RR spectra at 300 μJ pumping condition were faster than those at 10 μJ pumping condition, meaning that structural relaxation to the deoxy structure under the high pumping condition was faster than that in the low pumping condition. This pump energy dependence was also observed in a TRXL study of HbI.[42]

B. Comparisons between temporal changes in the RR bands obtained under high and low pumping conditions

Temporal changes in the RR bands of the ν(Fe–His), ν_7, $\delta(C_\beta C_c C_d)$, ν_7, ν_{16}, and ν_{32} modes obtained under low and high pumping conditions are shown in Fig. 3. These bands were selected because they exhibited prominent amplitudes of the frequency or intensity changes. The amplitudes of the changes were similar for the high and low pumping conditions, although the changes were faster under the high pumping condition compared to the low pumping condition.

The rates of the RR spectral changes differed between the photodissociated species of the single and double dissociations, as indicated by the apparent differences in the rates observed under the low and high pumping conditions. The observed spectral changes are linear combinations of the contributions of the singly and doubly dissociated species. However, the frequencies and intensities being apparently changed in a single phase, as shown in Fig. 3, due to small differences in the rates for the singly and doubly dissociated species. Therefore, all the spectral evolutions were fit by a single-exponential function of time, t, in the form $A\exp(-kt) + C$, where k, A, and C are the apparent rate constant of the spectral change, the magnitude of the spectral change, and the final value, respectively. The best fits are shown as solid lines in Fig. 3, and their parameters are presented in Table II.

The time-resolved RR spectra were measured under various pumping conditions, and the temporal changes were analyzed (Figs. S1 and S2 in the supplementary material). The dissociation fraction under each condition was determined based on the time-resolved spectra at 10 μs, as described in Sec. S2 of the supplementary material. The time-resolved spectra are linear combinations of the contributions of singly and doubly dissociated HbI calculated from the dissociation fraction described in Sec. S3 of the supplementary material. The rate constants of the spectral changes are plotted against a fraction of the spectral contribution of doubly dissociated HbI, f_2, shown in Fig. 4. The rate constants exhibited a linear relationship with f_2. The rate constants for the singly and doubly dissociated HbI were determined to be 0.05–0.90 and 1.65–3.08 μs^{-1}, respectively, by extrapolating the fit line to 0 and 1 for f_2.

Linear combinations of the contributions of the singly and doubly dissociated species were calculated using the determined rate

constants, f_2, and are shown as the broken lines in Fig. 3. The observed temporal changes were well expressed by linear combinations of the exponential functions with the rate constants of the singly and doubly dissociated species. This corroborates our analysis of the rate constants for the singly and doubly dissociated species shown in Fig. 4. It is notable that the spectral evolutions are well described by the single exponential function under the highest pumping condition, where the contribution of the doubly dissociated species was nearly 100%, indicating that the structural evolution following CO dissociation occurs in a single step in HbI in 20 ns–10 μs. This single-step transition of HbI is in sharp contrast to the three-step transitions observed for HbA. In HbA, three transitions in the order of 10, 100 ns, and 10 μs were observed for the frequency change of ν(Fe–His).[26,56–58] These temporal components were also observed in the ultraviolet RR spectral changes of Trp residues in HbA and are attributed to motions involving the proximal and distal helices as well as the subunit interface.[26,27]

C. Time-resolved RR spectra of the photodissociated HbI mutants

Figure 5 shows the time-resolved RR spectra of the HbI F97Y and F97L mutants. Temporal changes in the RR spectra were much faster and smaller in the mutants than those in the WT (Fig. S5 in the supplementary material), consistent with the results obtained by the TRXL studies on F97Y, which showed that F97Y exhibits faster kinetics than the WT and lacked the contraction of the two subunits observed in WT (although subunit rotation occurred).[42] Therefore,

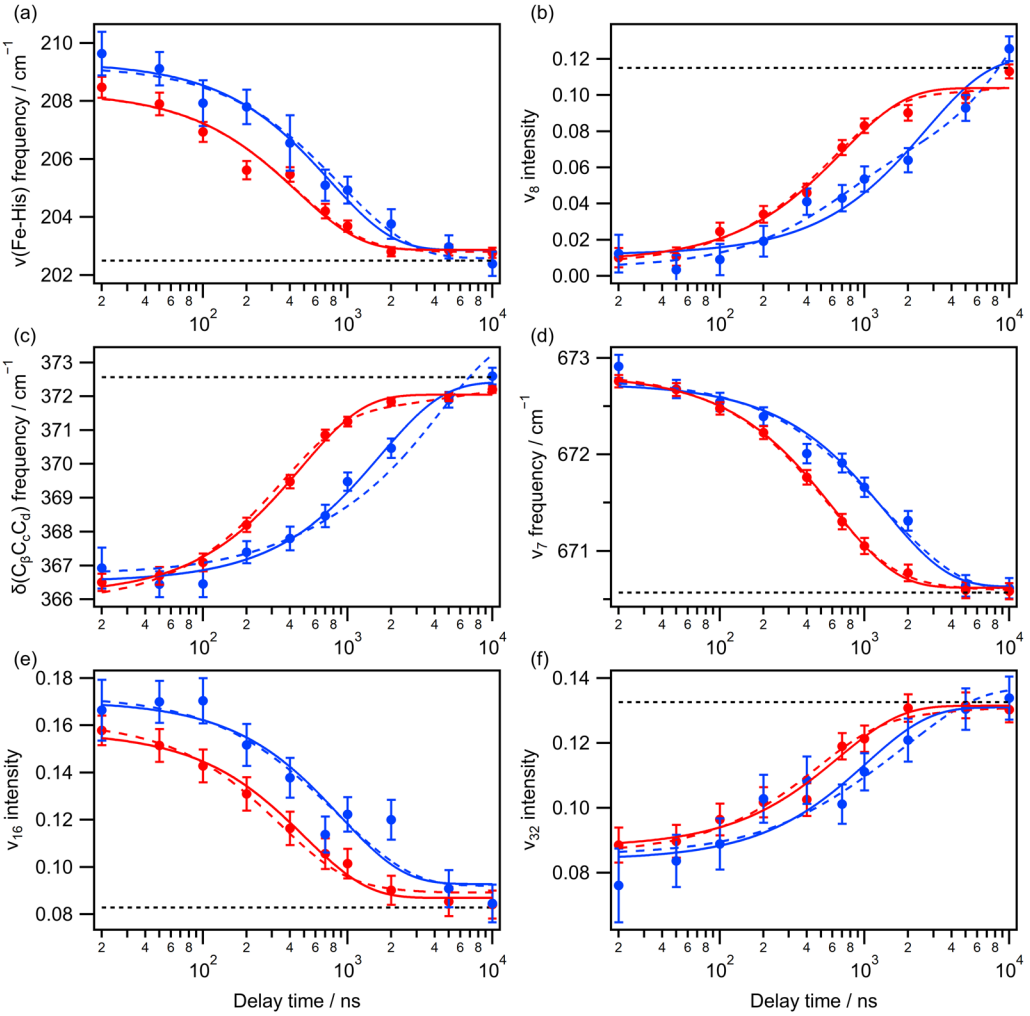

FIG. 3. Temporal changes of the band frequencies and intensities of WT HbI. (a) ν(Fe–His) frequency, (b) ν_8 intensity, (c) $\delta(C_\beta C_c C_d)$ frequency, (d) ν_7 frequency, (e) ν_{16} intensity, and (f) ν_{32} intensity. The red and blue markers show the frequencies and intensities under the pump energy of 300 μJ (dissociation fraction, 87.6%) and 10 μJ (22.4%), respectively. The solid lines indicate the best fits by a single exponential function. The broken lines show the linear combinations of the contributions from singly and doubly dissociated HbI. The dotted lines indicate the frequencies or intensities of the deoxy form. The intensities of the ν_8, ν_{16}, and ν_{32} bands are shown as relative values to the intensity of the ν_7 band.

TABLE II. Rate constants for the spectral evolution of the singly and doubly dissociated species of HbI.

	Rate constant (μs^{-1})	
Band	Singly dissociated species	Doubly dissociated species
Frequency		
ν(Fe–His)	0.873 ± 0.241	2.40 ± 0.26
$\delta(C_\beta C_c C_d)$	0.231 ± 0.118	2.85 ± 0.13
ν_7	0.549 ± 0.086	1.89 ± 0.09
Intensity		
ν_8	0.0520 ± 0.1440	1.65 ± 0.15
ν_{16}	0.896 ± 0.528	3.08 ± 0.56
ν_{32}	0.423 ± 0.282	2.22 ± 0.30

the spectral changes observed for WT can be largely attributed to the contraction of the two subunits, related to the flipping of Phe97 at the subunit interface of WT HbI.

D. Structural changes in the heme pocket

The observed spectral changes indicated that the structural evolution following CO dissociation occurs in a single step: the transient photodissociated species undergoes structural rearrangements directly to the deoxy structure. Accordingly, the structural differences between the CO-bound and deoxy forms are helpful for understanding the structural rearrangements following CO dissociation. A crystallographic study revealed the differences between the structures of the CO-bound and deoxy forms of HbI.[34] Figure 6 shows the comparison between the structures around the heme

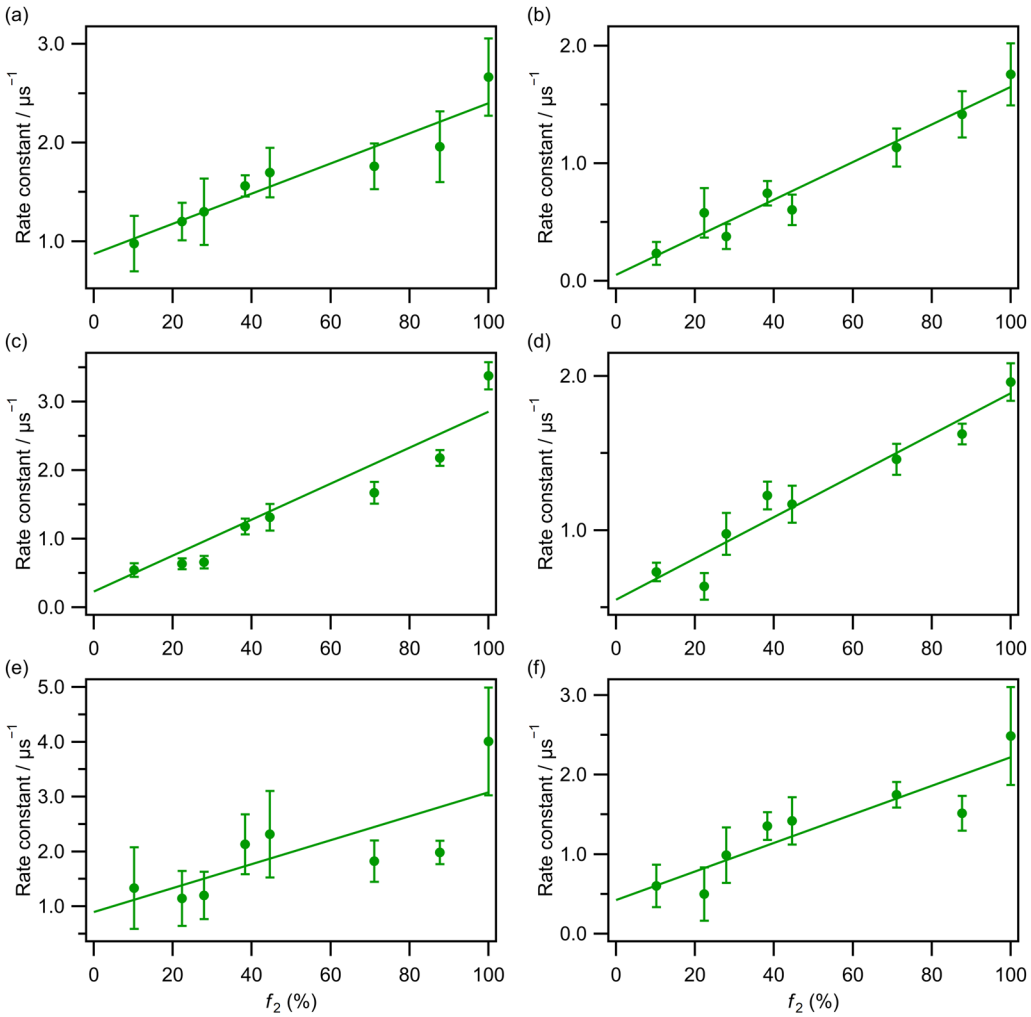

FIG. 4. Dependence of the rate constants for the temporal changes in the ν(Fe–His) frequency (a), ν_8 intensity (b), $\delta(C_\beta C_c C_d)$ frequency (c), ν_7 frequency (d), ν_{16} intensity (e), and ν_{32} intensity (f) on the fraction of the spectral contribution by doubly dissociated HbI. The solid lines show the best fit by a linear function.

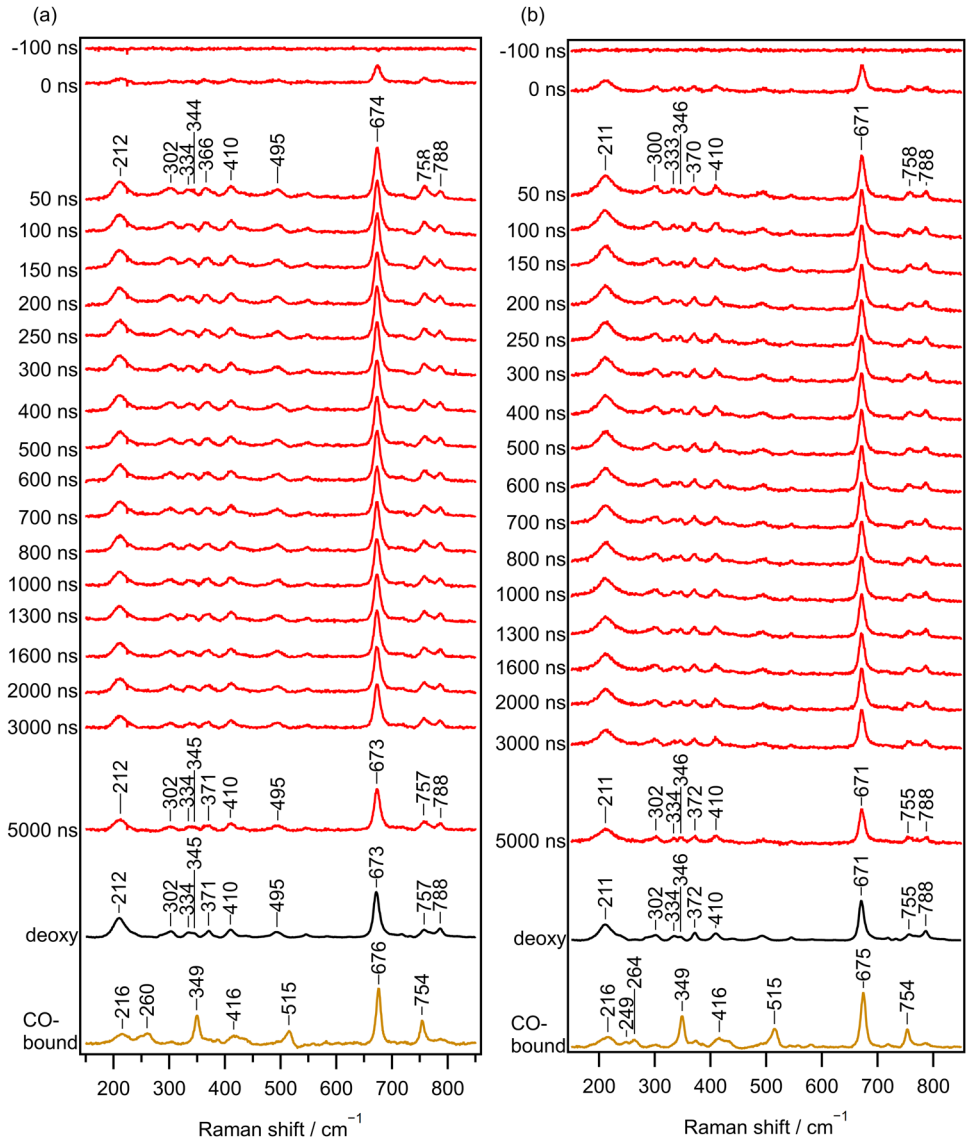

FIG. 5. Time-resolved RR spectra of the photodissociated F97Y (a) and F97L mutants (b). The pulse energy for the pump light was set to 20 μJ. The RR spectra of the CO-bound and deoxy forms of HbI are shown for comparison. The time-resolved spectra were generated by subtracting the probe-only spectrum from the pump–probe spectrum at each delay time.

group in the two forms, with the most striking difference being the orientation of the Phe97 side chain. The side chain is tightly packed against the heme group and proximal histidine (His101) in the deoxy form but extends from the heme pocket in the CO-bound form. The movement of the Phe97 side chain is coupled with the rearrangement of the F helix backbone. In addition, the tight packing of the Phe97 side chain in the heme pocket affects the position of the His101 side chain relative to the heme group. It is highly likely that these effects of the Phe97 side chain cause the frequency difference in the ν(Fe–His) mode between the deoxy form (203 cm^{-1}) and the CO-dissociated form at 50 ns (209 cm^{-1}).

The Fe–His bond is the sole covalent linkage between the heme and the globin. Thus, the ν(Fe–His) band is a useful marker of the heme pocket structure and is sensitive to the quaternary states of hemoglobins.[17,19,26–29] The ν(Fe–His) frequency of deoxy HbI (203 cm^{-1}) is much lower than those of the deoxy states of myoglobin or HbA, which are 215–220 cm^{-1}.[26] This low frequency of deoxy HbI indicates the high strain imposed on the covalent bond between the heme iron and His101 in deoxy HbI.[12,29] The downshift of the ν(Fe–His) band is ascribed to the change in the Fe–His bond strength accompanied by the F helix motion after CO dissociation.[11–13,15] In addition, there is a hydrogen bond between

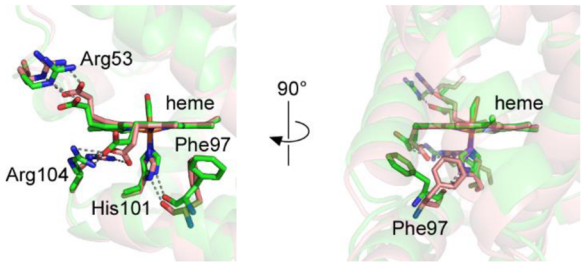

FIG. 6. Comparison of structures in the vicinity of the heme group of HbI in the CO-bound (green, PDB ID: 3SDH) and deoxy forms (pink, PDB ID: 4SDH).

N_δ of His101 and the main chain carbonyl of Phe97 (Fig. 6).[12,30] This hydrogen bond is proposed to partially stabilize the positive charge of the imidazole ring of the proximal histidine.[31] The length of the hydrogen bond increases with the intrusion of Phe97 after dissociation, which could decrease the strength of the Fe–His bond and consequently cause the ν(Fe–His) downshift.

Comparison of the results obtained for the WT and the mutants of HbI verifies that the ν(Fe–His) band shift is associated with the rotation of Phe97. The time-resolved RR spectra of the F97Y and F97L mutants did not show a ν(Fe–His) downshift (Fig. S5 in the supplementary material). The ν(Fe–His) band frequencies of the F97Y and F97L mutants remained unchanged in the time window of the measurements, similar to the frequency of WT HbI at 20 ns. Crystallographic studies revealed that the 97th residue of the two mutants did not undergo the side chain rotation observed in WT.[38] Moreover, comparative TRXL studies on F97Y and WT also showed that the 97th residue of F97Y did not show the flipping motion observed in WT.[42] The 97th Tyr side chain of F97Y extends into the interface, whereas the 97th Lys side chain of F97L mutant intrudes into the heme pocket.[14] The hydrogen bond between the His101 side chain and the main chain carbonyl at the 97th residue is almost of the same length as that in the CO-bound WT HbI.[13,14] Accordingly, the effects of the 97th residue on the His101 side chain would not change upon CO dissociation in the F97 mutants.

The increase in the intensity of the ν_8 band following CO dissociation is explained well by the tightening of the atomic contacts between the side chains of Phe97 and His101 upon Phe97 intrusion into the heme pocket. The atomic displacements between the electronic ground and excited states have a nonzero component along the ν_8 coordinate because the ν_8 mode is the in-plane stretching mode between the iron and pyrrole nitrogen atoms. Thus, the RR intensity of the ν_8 band is related to its in-plane vibrational character and increases when the iron atom approaches the porphyrin plane. The intrusion of the Phe97 side chain changes the iron position relative to the pyrrole nitrogen atom by affecting the position of the His101 side chain. Thus, the change in the iron position results in an increase in the intensity of the ν_8 band. The rate constants for the ν_8 intensity changes were smaller than those for the changes in other modes. The ν_8 mode is the only vibrational mode that includes relative motions between the heme iron and heme. The intensity change of the ν_8 band may suggest that the iron-histidine unit approaches the heme plane more slowly than the other structural changes in heme.

The intensity of the ν_{16} band at 756 cm^{-1} in the time-resolved spectra of the WT at 20 ns increased prominently as the delay time increased. This band is due to a symmetric pyrrole ring deformation mode that involves a large contribution from the displacement of the nitrogen atom on the pyrrole rings[50,52] and can thus be sensitive to steric interactions between the heme macrocycle and amino acid residues in van der Waals contact with it. Accordingly, the deligation-induced movement of Phe97 into the heme pocket likely caused the intensity change in the ν_{16} band. In contrast to the WT, the intensity decrease of the ν_{16} band was small for the F97Y and F97L mutants (Fig. S5 in the supplementary material). The ν_{16} band intensities of the F97Y and F97L mutants were similar to those of the WT at 20 ns and 10 μs, respectively, demonstrating that the intensity of the ν_{16} band correlates with the van der Waals contacts between the 97th side chain and the heme.

The ν_{32} mode is an asymmetric pyrrole ring deformation mode and has large contributions from the vinyl groups.[59,60] In the deoxy state, the side chain of Phe97 pushes the heme group and the side chain of His101, resulting in changes in the interactions between the vinyl groups and the heme pocket. The decrease in the intensity of the ν_{32} band is likely due to the movement of the heme group in the heme pocket induced by the Phe97 intrusion.

The ν_7 mode is a symmetric pyrrole ring deformation mode and involves contributions from the propionate groups.[55] Thus, the frequency of the ν_7 band is attributable to changes in the interactions of the propionates. Another difference in the F helix, where Phe97 and His101 are located, was observed in the salt bridges between the side chain of Arg104 and the propionate groups of the heme. Both carboxylate oxygens of the heme propionates form salt bridges with the Arg104 side chain in the deoxy form, whereas salt bridges are formed between Arg104 and one of the carboxylate oxygens of the heme propionates in the CO-bound form (Fig. 6). The other propionate group also exhibited a difference in its salt bridge to Arg53. Two nitrogen atoms of the Arg53 side chain form salt bridges with heme propionate in the deoxy form, while a salt bridge is formed between a nitrogen atom of the Arg53 side chain and a heme propionate in the CO-bound form. These differences in the propionate groups cause a frequency difference in the $\delta(C_\beta C_c C_d)$ mode between the deoxy and CO-bound forms.

E. Structural changes in the subunit interface

Interfacial water molecules reportedly play a key role in the allosteric process of HbI[32–34,36] since the two heme groups are indirectly hydrogen-bonded to each other at the propionates through water molecules. The crystallographic data show that the CO-bound and deoxy forms have prominent differences in the structure of the interfacial water cluster and the number of water molecules constituting the water cluster, resulting from structural differences in the heme and globin.[32–34,36] Figure 7 shows a comparison of the positions of the interfacial water molecules and the structures of the heme in the CO-bound and deoxy states. These structural changes result from the deligation-induced structural changes in the heme and globin. The propionate groups undergo large structural changes accompanied by rearrangement of the water cluster. It is highly likely that such rearrangements caused the spectral changes in the $\delta(C_\beta C_c C_d)$ and ν_7 bands, in addition to the contributions of the changes in the salt bridges with Arg53 and Arg104.

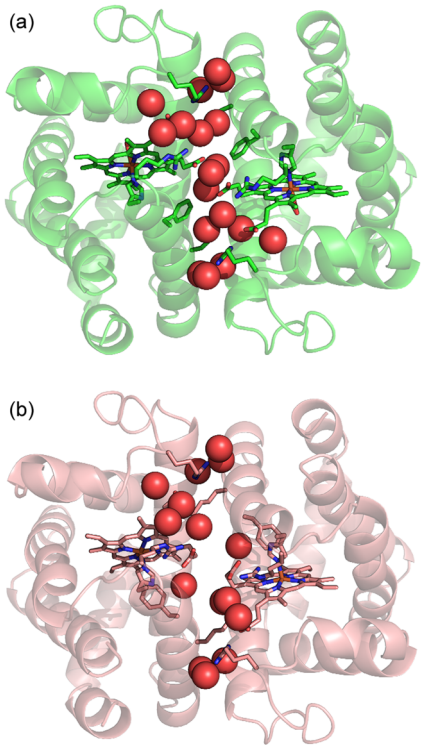

FIG. 7. Comparison of the positions of the interfacial water molecules of HbI in the CO-bound [(a), PDB ID: 3SDH] and deoxy forms [(b), PDB ID: 4SDH]. Oxygen atoms of the water molecules located 3.25 Å from the oxygen atoms of the heme propionate, an N^{η} atom of Arg53, or an N^{η} atom of Arg104, shown as red spheres.

Intriguingly, the rate constants of the $\delta(C_\beta C_c C_d)$ and ν_7 spectral changes due to the rearrangements of the water cluster were similar to those for the rearrangement of the heme pocket, suggesting that the heme pocket and the subunit interface nearly synchronously undergo structural rearrangements.

Kim *et al.* investigated the deligation-induced protein dynamics of HbI by measuring time-resolved x-ray solution scattering.[42] The data showed that one subunit rotated relative to the second subunit by 3.4°, identical to the angle observed in the protein crystallographic data. The corresponding rotational angle was slightly smaller in the F97Y mutant (3.0° in F97Y vs 3.5° in WT). They determined that the time constants of the quaternary change were 730 ± 120 ns and 5.6 ± 0.8 μs for the doubly and singly dissociated species of WT. The time constants for the ν(Fe–His), ν_8, $\delta(C_\beta C_c C_d)$, ν_7, ν_{16}, and ν_{32} bands observed in the present study are comparable to those obtained from the x-ray solution scattering study. This similarity shows that the structural changes of the heme pocket are synchronous to the rearrangements of the water cluster and are accompanied by the quaternary structural change.

F. Differences between the CO deligation-induced structural dynamics of HbI and HbA

The observed structural changes following CO dissociation from HbI were different from those of HbA in several respects. First, the number of structural transitions following CO dissociation was different between the two hemoglobins. The structural transition occurred in the single step for HbI, whereas three steps involving motions in the proximal and distal helices and the subunit interface were observed for HbA.[26,56–58] Second, spectral changes that were not observed in HbA were observed in HbI: the frequencies of the $\delta(C_\beta C_c C_d)$ and ν_7 bands changed in the time-resolved RR spectra for HbI but remained unchanged in the spectra for HbA.[58]

These differences are likely due to differences in the assembly of the subunits. The interacting sites are different in the two hemoglobins despite the subunit structures being very similar. The subunits contact each other through the E and F helices in HbI, whereas in HbA, the subunits contact each other through the C helix and the FG corner, which undergo structural rearrangement in the quaternary change. Comparison between the protein structures of HbI and HbA are shown in Fig. S6. The heme groups face each other in HbI, while the heme groups are separated by more than 20 Å in HbA. Therefore, it is likely that structural changes in the heme pockets and the subunit interface occur synchronously in HbI but change in a stepwise fashion in HbA. The connections of the heme propionates in another subunit of HbI mediated by interfacial water result in the observed frequency changes of the $\delta(C_\beta C_c C_d)$ and ν_7 bands upon the quaternary transition of HbI.

G. Deligation number dependence of the structural dynamics of photodissociated HbI

The present data clearly show that the rate of the structural transition from the photodissociated species to the equilibrium-deligated species is different between singly and doubly dissociated HbI. The time-resolved RR spectra at 20 ns are similar in Figs. 2(a) and 2(b). In addition, the magnitudes of the spectral changes are similar between the high and low pumping conditions, as shown in Fig. 3. These similarities indicate that the heme pocket structures at the start and end of the transition for the singly dissociated species are similar to those for the doubly dissociated species. Regardless of these similarities, the rates of the structural changes for the singly and doubly dissociated species depend on the dissociation number of the ligand. Accordingly, the deligation-induced structural changes in the heme groups and heme pockets in one subunit depend on the structure of the other subunit. This intersubunit coupling increases the activation energy for the structural transition in the singly dissociated species compared to that in the doubly dissociated species, suggesting that the transient state for the asymmetric transition is less stable than the symmetric transition in the homodimeric subunits of HbI. That the protein structure of HbI favors symmetric forms is associated with its positive cooperativity upon oxygen association/dissociation.

IV. CONCLUSIONS

The present study revealed the structural dynamics of the heme and heme pockets in HbI following CO dissociation using time-resolved RR spectroscopy. The time-resolved spectra showed that the Fe–His bond, the relative position of heme in the pocket, and hydrogen bonds between heme and interfacial water are altered upon ligand dissociation. The similarity in the rates of these changes

and the quaternary change indicate that the changes in the heme pocket are synchronous with the relative rotation of the subunits. Faster transition from the photodissociated form to the equilibrium-deligated form in the doubly dissociated species compared to that in the singly dissociated form is associated with the intersubunit coupling underlying the positive cooperativity of HbI. Photodissociated HbI underwent rearrangement of the heme propionates, whereas this rearrangement was not observed in photodissociated HbA as the rearrangement is associated with different assemblies of the structurally similar subunits and different quaternary changes. These findings help further characterize the protein dynamics regulating the allosteric pathway of the hemoglobins composed of globin-folded subunits.

SUPPLEMENTARY MATERIAL

See the supplementary material for the temporal changes of the band frequencies and intensities under various pumping conditions, procedures for determining the dissociation fraction, contributions of the photodissociated heme involved in the singly and doubly dissociated HbI to the time-resolved RR spectra, the temporal changes of the band frequencies and intensities of the HbI mutants, and comparison between the protein structures of HbI and human adult hemoglobin.

ACKNOWLEDGMENTS

This work was supported by the Support for Pioneering Research Initiated by the Next Generation from Japan Science and Technology Agency (Grant No. JPMJSP2138, X.G.) and Grants-in-Aid for Scientific Research from the JSPS (Grant Nos. JP20H02693, Y.M., and JP23H00285, Y.M.). This work was also supported by the Institute for Basic Science (Grant No. IBS-R033).

AUTHOR DECLARATIONS

Conflict of Interest

The authors have no conflicts to disclose.

Author Contributions

Xiang Gao: Data curation (lead); Formal analysis (lead); Investigation (lead); Visualization (equal); Writing – original draft (lead). **Misao Mizuno**: Data curation (equal); Formal analysis (equal); Investigation (supporting); Writing – review & editing (supporting). **Haruto Ishikawa**: Data curation (equal); Formal analysis (equal); Investigation (supporting); Writing – review & editing (supporting). **Srinivasan Muniyappan**: Investigation (supporting). **Hyotcherl Ihee**: Conceptualization (equal); Funding acquisition (supporting); Resources (equal); Writing – review & editing (supporting). **Yasuhisa Mizutani**: Conceptualization (equal); Data curation (equal); Funding acquisition (lead); Project administration (equal); Validation (lead); Writing – review & editing (lead).

DATA AVAILABILITY

The data that support the findings of this study are available from the corresponding author upon reasonable request.

REFERENCES

[1] J. Monod, J. Wyman, and J.-P. Changeux, J. Mol. Biol. **12**, 88 (1965).
[2] D. E. Koshland, Jr., G. Némethy, and D. Filmer, Biochemistry **5**, 365 (1966).
[3] J.-P. Changeux and S. J. Edelstein, Science **308**, 1424 (2005).
[4] E. Antonini and M. Brunori, Annu. Rev. Biochem. **39**, 977 (1970).
[5] E. Antonini and M. Brunori, *Hemoglobin and Myoglobin in Their Reactions with Ligands* (North-Holland Publishing Company, Amsterdam, 1971).
[6] R. E. Dickerson and I. Geis, *Hemoglobin: Structure, Function, Evolution and Pathology* (Benjamin-Cummings Publishing Company, Menlo Park, 1983).
[7] W. A. Eaton *et al.*, Nat. Struct. Biol. **6**, 351 (1999).
[8] B. Shaanan, J. Mol. Biol. **171**, 31 (1983).
[9] G. Fermi *et al.*, J. Mol. Biol. **175**, 159 (1984).
[10] J. W. Petrich, C. Poyart, and J. L. Martin, Biochemistry **27**, 4049 (1988).
[11] X. Ye, A. Demidov, and P. M. Champion, J. Am. Chem. Soc. **124**, 5914 (2002).
[12] T. Bücher and J. Kaspers, Biochim. Biophys. Acta **1**, 21 (1947).
[13] Q. H. Gibson *et al.*, J. Biol. Chem. **261**, 10228 (1986).
[14] L. J. Parkhurst, Annu. Rev. Phys. Chem. **30**, 503 (1979).
[15] E. Antonini *et al.*, J. Biol. Chem. **259**, 6730 (1984).
[16] J. S. Olson and G. N. Phillips, Jr., J. Biol. Chem. **271**, 17593 (1996).
[17] T. Kitagawa, in *Biological Applications of Raman Spectroscopy*, edited by T. G. Spiro (John Wiley & Sons, New York, 1987), p. 97.
[18] D. Rousseau and J. Friedman, in *Biological Applications of Raman Spectroscopy*, edited by T. G. Spiro (John Wiley & Sons, New York, 1988), Vol. 3, p. 133.
[19] T. G. Spiro and R. S. Czernuszewicz, *Methods Enzymol* (Academic Press, 1995), p. 416.
[20] S. Kaminaka, T. Ogura, and T. Kitagawa, J. Am. Chem. Soc. **112**, 23 (1990).
[21] S. Kaminaka and T. Kitagawa, J. Am. Chem. Soc. **114**, 3256 (1992).
[22] M. Nagai *et al.*, J. Biol. Chem. **270**, 1636 (1995).
[23] M. Nagai *et al.*, J. Mol. Struct. **379**, 65 (1996).
[24] K. R. Rodgers *et al.*, J. Am. Chem. Soc. **114**, 3697 (1992).
[25] K. R. Rodgers and T. G. Spiro, Science **265**, 1697 (1994).
[26] V. Jayaraman *et al.*, Science **269**, 1843 (1995).
[27] G. Balakrishnan *et al.*, J. Mol. Biol. **340**, 843 (2004).
[28] T. W. Scott and J. M. Friedman, J. Am. Chem. Soc. **106**, 5677 (1984).
[29] J. M. Friedman, Science **228**, 1273 (1985).
[30] S. Dasgupta and T. G. Spiro, Biochemistry **25**, 5941 (1986).
[31] E. Chiancone *et al.*, J. Mol. Biol. **152**, 577 (1981).
[32] W. E. Royer, W. A. Hendrickson, and E. Chiancone, J. Biol. Chem. **264**, 21052 (1989).
[33] W. E. Royer, W. A. Hendrickson, and E. Chiancone, Science **249**, 518 (1990).
[34] W. E. Royer, J. Mol. Biol. **235**, 657 (1994).
[35] P. J. Condon and W. E. Royer, Jr., J. Biol. Chem. **269**, 25259 (1994).
[36] W. E. Royer *et al.*, Proc. Natl. Acad. Sci. U. S. A. **93**, 14526 (1996).
[37] J. E. Knapp and W. E. Royer, Biochemistry **42**, 4640 (2003).
[38] J. E. Knapp *et al.*, Biochemistry **44**, 14419 (2005).
[39] E. Chiancone *et al.*, J. Biol. Chem. **268**, 5711 (1993).
[40] J. C. Nichols, W. E. Royer, and Q. H. Gibson, Biochemistry **45**, 15748 (2006).
[41] J. Choi *et al.*, ChemPhysChem **11**, 109 (2010).
[42] K. H. Kim *et al.*, J. Am. Chem. Soc. **134**, 7001 (2012).
[43] J. G. Kim *et al.*, Struct. Dyn. **3**, 023610 (2016).
[44] C. Yang *et al.*, Int. J. Mol. Sci. **19**, 3633 (2018).
[45] H. Kim *et al.*, J. Phys. Chem. B **124**, 1550 (2020).
[46] M. Choi *et al.*, Chem. Sci. **12**, 8207 (2021).
[47] Y. Lee *et al.*, Nat. Commun. **12**, 3677 (2021).
[48] C. M. Summerford *et al.*, Protein Eng., Des. Sel. **8**, 593 (1995).

[49]K. Yamada, H. Ishikawa, and Y. Mizutani, J. Phys. Chem. B **116**, 1992 (2012).
[50]M. Abe, T. Kitagawa, and Y. Kyogoku, J. Chem. Phys. **69**, 4526 (1978).
[51]T. Kitagawa, M. Abe, and H. Ogoshi, J. Chem. Phys. **69**, 4516 (1978).
[52]X. Y. Li *et al.*, J. Phys. Chem. **94**, 47 (1990).
[53]X. Y. Li *et al.*, J. Am. Chem. Soc. **111**, 7012 (1989).
[54]D. L. Rousseau *et al.*, J. Biol. Chem. **268**, 5719 (1993).
[55]S. Hu, K. M. Smith, and T. G. Spiro, J. Am. Chem. Soc. **118**, 12638 (1996).
[56]K. Yamada *et al.*, J. Phys. Chem. B **117**, 12461 (2013).
[57]S. Chang *et al.*, Chem. Phys. **469–470**, 31 (2016).
[58]S. Chang *et al.*, Phys. Chem. Chem. Phys. **20**, 3363 (2018).
[59]S. Choi *et al.*, J. Am. Chem. Soc. **104**, 4345 (1982).
[60]D. L. Rousseau *et al.*, J. Biol. Chem. **258**, 1740 (1983).